Cone Penetration Testing 2022 – Gottardi & Tonni (eds)

Methodology for obtaining true cone bearing estimates from blurred and noisy measurements

Erick Baziw & Gerald Verbeek
Baziw Consulting Engineers Ltd., Vancouver, Canada

ABSTRACT: Cone penetration testing (CPT) is an important and widely used geotechnical *in-situ* test for assessing soil properties and mapping soil profiles. CPT consists of pushing at a constant rate an electronic cone into penetrable soils and recording the resistance to the cone tip or cone bearing (q_m). These values (after correction for the pore water pressure to get q_t) are utilized to characterize the soil profile along with measured sleeve friction and pore pressure. The q_m measurements can have significant fluctuations when penetrating sandy, silty gravelly soils, resulting in "high" peaks due to interbedded gravels and stones and "low" peaks due to softer materials or local pore pressure build-up. Furthermore, the q_m values are blurred and/or averaged which results in the inability to identify thin layers and the distortion of the soil profile characterization. Baziw Consulting Engineers has invested considerable resources in addressing these two q_m measurement challenges. The q_mKF algorithm was developed to address the additive measurement noise. In this case the dynamics of q_m are modeled within a state-space mathematical formulation and a Kalman filter is then utilized to obtain optimal estimates of q_m. The q_mHMM algorithm implements a hidden Markov model smoother so that true cone bearing are obtained from the averaged/blurred q_m values. This paper outlines the integration of the q_mKF and q_mHMM algorithms and demonstrates the performance first with test bed simulations (to show the functionality of the algorithm) and then through the analysis of various actual q_m data sets.

1 INTRODUCTION

1.1 *Cone bearing measurements*

The Cone Penetration Test (CPT) is a geotechnical in-situ tool which is utilized to identify and characterize sub-surface soils (Lunne et al., 1997; Robertson, 1990; ASTM D6067, 2017). In CPT a cone penetration rig pushes the steel cone vertically into the ground at a standard rate and data are recorded at regular intervals during penetration. The cone has electronic sensors to measure penetration resistance at the tip (q_m) and friction in the shaft (friction sleeve) during penetration. A CPT probe equipped with a pore-water pressure sensor is called a piezo-cone (CPTU cones). For piezo-cones with the filter element right behind the cone tip (the so-called u_2 position) it is standard practice to correct the recorded tip resistance for the impact of the pore pressure on the back of the cone tip. This corrected cone tip resistance is normally referred to as q_t. The distortions which effect the cone tip measurements are two-fold: 1) the cone tip resistance are smoothed/averaged (Boulanger and DeJong, 2018; Baziw and Verbeek, 2021a) where cone tip values measured at a particular depth are affected by values above and below the depth of interest, and 2) the cone bearing measurements are susceptible to anomalous peaks and troughs due to the relatively small diameter cone tip penetrating sandy, silty and gravelly soils (Baziw and Verbeek, 2021b).

1.2 *Cone bearing smoothing/averaging*

The measured cone resistance at a particular depth is an averaged/smoothed measurement of the true values q_v above and below the depth of interest (Boulanger and DeJong, 2018; Robertson, 1990; Baziw and Verbeek, 2021a, 2021b). Mathematically the measured cone tip resistance q_m is described as (Baziw and Verbeek, 2021a)

$$q_m(d) = \sum_{j=1}^{60\times\left(\frac{d_c}{\Delta}\right)} w_c(j) \times q_v\left(\Delta_{qm} + j\right) + v(d)$$
$$\Delta_{qm} = (d - \Delta_{wm}), \Delta_{wm} = 30 \times \left(\frac{d_c}{\Delta}\right) \quad (1)$$

where
d the cone depth
d_c the cone tip diameter
Δ_{qm} the q_m sampling rate
$q_m(d)$ the measured cone tip resistance
$q_v(d)$ the true cone tip resistance (prior to pore water pressure correction)

DOI: 10.1201/9781003308829-9

$w_c(d)$ the $q_v(d)$ averaging function
$v(d)$ additive noise, generally taken to be white with a Gaussian pdf

In equation (1) it assumed that w_c averages q_v over 60 cone diameters centered at the cone tip. Boulanger and DeJong (Boulanger and DeJong, 2018) outline how to calculate w_c below (after correcting the equation for w_1 (Baziw and Verbeek, 2021a)):

$$w_c = \frac{w_1 w_2}{\sum w_1 w_2} \tag{2a}$$

$$w_1 = \frac{C_1}{1 + \left|\left(\frac{z'}{z'_{50}}\right)^{m_z}\right|} \tag{2b}$$

$$w_2 = \sqrt{\frac{2}{1 + \left(\frac{q_{t,z'}}{q_{t,z'=0}}\right)^{m_q}}} \tag{2c}$$

where:
z' the depth relative to the cone tip normalized by the cone diameter
z'_{50} the normalized depth relative to the cone tip where $w_1 = 0.5\ C_1$
The cone penetration averaging function w_c for varying $q_{t,z'}/q_{t,z'=0}$ ratios is illustrated in Figure 1.

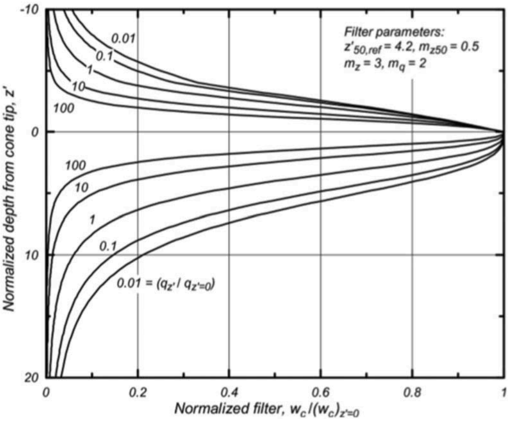

Figure 1. Schematic of thin layer effect for a sand layer embedded in a clay layer (Boulanger and DeJong, 2018).

1.3 *Cone bearing measurement noise*

The smoothed/averaged cone bearing measurement q_m given by eq. (1) can also contain sharp anomalous and spurious peaks and troughs (Lunne, Robertson and Powell, 1997)

These anomalous and spurious cone bearing measurements are due to the relatively small diameter cone tip penetrating sandy, silty and gravelly soils. As illustrated in Figure 2, the "high" peaks result from the penetration of interbedded gravels and stones and the "low" peaks results from the penetration of softer materials or local pore pressure build-up. Figure 3 illustrates an example of a cone bearing profile which contains significant anomalous/spurious q_m data from approximate depths 10m to 18m and 22m to 30m. There is also significant pore pressure variability at these depths.

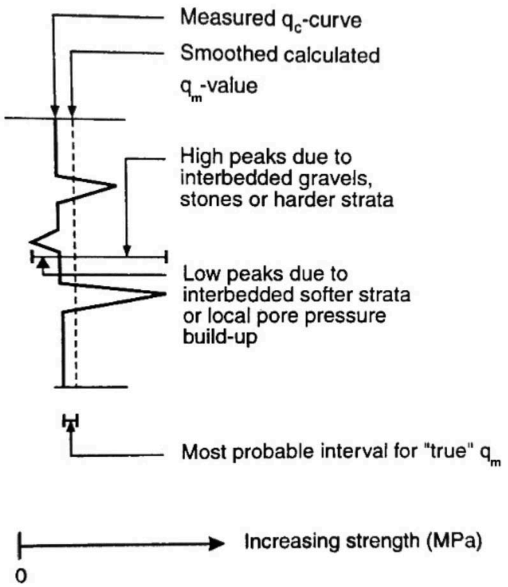

Figure 2. Schematic of anomalous/spurious cone bearing data (after Mortensen and Sorensen, 1991).

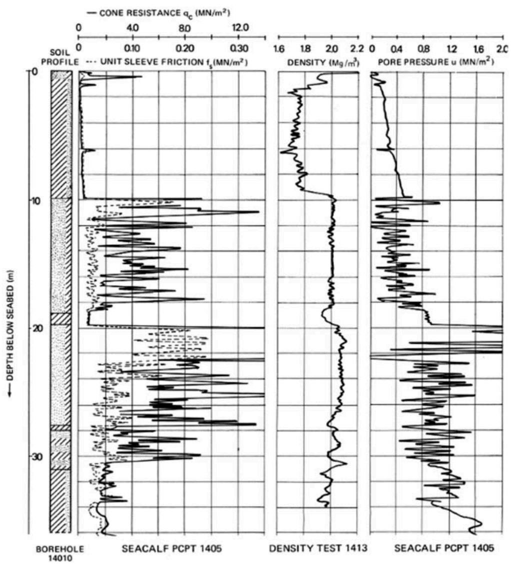

Figure 3. Combined results of piezocone test and nuclear density test at Gullfaks C in the North Sea (Tjelta et al. 1985).

2 FILTER FORMULATION

2.1 *qmHMM algorithm formulation*

The initial algorithm developed by Baziw and Verbeek (2021a) (the so called q_m*HMM-IFM*) to address the smoothing/averaging of cone bearing measurements (eq. (1)) combined a Bayesian recursive estimation (BRE) Hidden Markov Model (HMM) filter with Iterative Forward Modelling (IFM) parameter estimation in a smoother formulation. The q_m*HMM-IFM* provided estimates of the true q_v values from the measured blurred values. In recent modifications and enhancements of the q_m*HMM-IFM* it was possible to drop the IFM portion of the algorithm. This was predominantly accomplished by refining the HMM filter parameters.

The HMM filter (also termed a grid-based filter) has a discrete state-space representation and has a finite number of states (Arulampalam et al., 2002). In the HMM filter the posterior PDF is represented by the delta function approximation as follows:

$$p(x_{k-1}|z_{1:k-1}) = \sum_{i=1}^{N_s} w^i_{k-1\backslash k-1}\delta\left(x_{k-1} - x^i_{k-1}\right) \quad (3)$$

where x^i_{k-1} and $w^i_{k-1|k-1}$, $i = 1,\ldots,N_s$, represent the fixed discrete states and associated conditional probabilities, respectively, at time index k-1, and N_s the number of particles utilized. In the case of the q_mHMM algorithm the HMM discrete states represent possible q_v values where

Table 1. HMM filtering algorithm.

Step	Description	Mathematical Representation
1	Initialization (k=0) – initialize particle weights.	e.g.,$w^i_k \sim 1/N_s$, i = $1,\ldots,N_s$ (4)
2	Prediction - predict the weights.	$w^i_{k\backslash k-1} = \sum_{j=1}^{N_s} w^j_{k-1\backslash k-1} p\left(x^i_k|x^j_{k-1}\right)$ (5)
3	Update - update the weights.	$w^i_{k\backslash k} = \frac{w^i_{k\backslash k-1} p\left(z_k|x^i_k\right)}{\sum_{j=1}^{N_s} w^j_{k\backslash k-1} p\left(z_k|x^j_k\right)}$ (6)
4	Obtain optimal minimum variance estimate of the state vector and corresponding error covariance.	$\hat{x}_k \approx \sum_{i=1}^{N_s} w^i_{k\|k} x^i_k$ & (7)
5	Let k = k+1 & iterate to step 2.	$P_{\hat{x}_k} \approx \sum_{i=1}^{N_s} w^i_{k\|k}\left(x^i_k - \hat{x}_k\right)\left(x^i_k - \hat{x}_k\right)^T$

In the above equations it is required that the likelihood pdf $p(z_k|x^i_k)$ and the transitional probabilities $p(x^i_k|x^j_{k-1})$ be known and specified.

maximum, minimum and resolution values are specified. The HMM governing equations are outlined in Table 1.

The q_mHMM algorithm implements a BRE smoother. BRE smoothing uses all measurements available to estimate the state of a system at a certain time or depth in the q_v estimation case (Arulampalam et al., 2002; Baziw and Verbeek, 2021a; Gelb, 1974). This requires both a forward and backward filter formulation. The forward HMM filter ($\hat{q}^F_k$) processes measurement data (q_m) above the cone tip ($j = 1$ to $30 \times \left(\frac{d_c}{\Delta}\right)$) in (1)). Next the backward HMM filter ($\hat{q}^B_k$) is implemented, where the filter recurses through the data below the cone tip ($j = 30 \times \left(\frac{d_c}{\Delta}\right)$to $60 \times \left(\frac{d_c}{\Delta}\right)$ in (1)) starting at the final q_m value. The optimal estimate for $q_v$is then defined as

$$\hat{q}^v_k = \left(\hat{q}^F_k + \hat{q}^B_k\right)/2 \quad (8)$$

where the index k represents each q_m measurement.

In both the forward and backward HMM filter formulation a bank of discrete $q_v$values ($i = 1$ *to* N) varying from low (q_{tL}) to high (q_{tH}) and a corresponding q_t resolution q_{tR} is specified. The required number of fixed grid HMM states is given as $N_S = (q_{tH} - q_{tL})/q_{tR}$. In Table 1 the notation of the states x^i is mapped to q^i to reflect the bank of $q_t$values.

In the q_mHMM forward and backward filter formulation the transitional probabilities (i.e., $p\left(x^i_k|x^j_{k-1}\right)$ or $p\left(q^i_k|q^j_{k-1}\right)$ for each HMM state (i.e., discrete cone tip, $q^{\prime i}$) is set equal due to the fact that there is equal probability of moving from a current cone tip value to any other value between the range q_{tL} to q_{tH}. The likelihood PDF $p(z_k|q^i_k)$ in the HMM filter outlined in Table 1 is calculated based upon an assumed Gaussian measurement error as follows:

$$p(z_k|q^i_k) = \frac{1}{\sqrt{2\pi\sigma}} e^{\left[-\frac{\left(q_c(d)-z^i_k\right)}{2\sigma^2}\right]} \quad (9)$$

where $\sigma^2$is the variance of the measurement noise. Baziw and Verbeek (2021a) outline the details of the q_mHMM algorithm forward and backward filter formulation.

2.2 *qmKF algorithm formulation*

The Kalman Filter (Gelb, 1974) is an optimal (least squares) recursive filter which is based on state-space formulations of physical problems. Application of this filter requires that the physical problem be modified by a set of first order differential equations which, with initial conditions, uniquely define the system behaviour. The filter utilizes knowledge

Table 2. KF governing equations.

Description	Mathematical Representation	
System equation	$x_k = F_{k-1}x_{k-1} + G_{k-1}u_{k-1}$	(10)
Measurement equation	$z_k = H_k x_k + v_k$	(11)
State estimate extrapolation	$\hat{x}_{k\|k-1} = F_{k-1}\hat{x}_{k-1\|k-1}$	(12)
Error cov. extrapolation	$P_{k\|k-1} = F_{k-1}P_{k-1\|k-1}F_{k-1}{}^{T}$	(13)
Measurement extrapolation	$G_{k-1}Q_{k-1\|k-1}G_{k-1}{}^{T}$ $\hat{z}_k = H_{k-1}\hat{x}_{k\|k-1}$	(14)
Innovation	$\Delta_k = z_k - \hat{z}_k$	(15)
Variance of innovation	$S_k = H_k P_{k\|k-1} H_k^T + R_k$	(16)
Kalman gain matrix	$K_k = P_{k\|k-1} H_k (S_k)^{-1}$	(17)
State estimate update	$\hat{x}_{k\|k} = \hat{x}_{k\|k-1} + K_k \Delta_k$	(18)
Error covariance update	$P_{k\backslash k} = [I - K_k H_k] P_{k\|k-1}$	(19)

In (10) and (11) $\boldsymbol{v}_k$ and $\boldsymbol{u}_k$ are *i.i.d* Gaussian zero mean white noise processes with variances of $\boldsymbol{Q}_k$ and $\boldsymbol{R}_k$, respectively (i.e.,$v_k \sim N(0, R_k)$ and $u_k \sim N(0, Q_k)$).

of system and measurement dynamics, assumed statistics of system noises and measurement errors and statistical information about the initial conditions.

Table 2 outlines the KF governing equations. In Table 2 $\boldsymbol{x_k}$ denotes the state to be estimated, $\boldsymbol{F}_{k\text{-}1}$ denotes the state transition matrix which describes the system dynamics, $\boldsymbol{u}_{k\text{-}1}$ the process or system noise (model uncertainty), $\boldsymbol{G}_{k\text{-}1}$ describes the relationship between $\boldsymbol{x_k}$ and $\boldsymbol{u}_{k\text{-}1}$, and $\boldsymbol{H}_k$ the relationship between the state and the available measurement (measured cone resistance q_m). The KF can be applied to problems with linear time-varying systems and with non-stationary system and measurement statistics. The KF can be implemented for estimation, smoothing and prediction.

The motivation of implementing the KF for the optimal removal of spurious cone bearing measurements is that it can use any number, combination and sequence of external measurements. For example, it is envisioned measurements from the vane shear test undrained strength could be incorporated within q_m*KF* algorithm based upon empirical correlations. Furthermore, it also fits into our goal of implementation of data fusion techniques into CPTU and SCPT.

Baziw and Verbeek (2021B) present a thorough outline of the q_m*KF* algorithm. For completeness, the KF state and measurement equations are described below.

2.3 *System model*

To specify the q_m*KF* systems equations in the standard KF state-space form, the following states need to be defined

$$\begin{bmatrix} x_1 \\ x_2 \\ x_3 \end{bmatrix} \equiv \begin{bmatrix} q_m\ conebearingposition \\ q_m\ conebearingvelocity \\ q_m\ conebearingacceleration \end{bmatrix} \tag{20}$$

The discrete system equation (eq. (10)) is given as

$$\begin{bmatrix} x_{1k+1} \\ x_{2k+1} \\ x_{3k+1} \end{bmatrix} = \begin{bmatrix} 1 & \Delta & \Delta^2/2 \\ 0 & 1 & \Delta \\ 0 & 0 & a_w \end{bmatrix} \begin{bmatrix} x_{1k} \\ x_{2k} \\ x_{3k} \end{bmatrix} + \begin{bmatrix} 0 \\ 0 \\ b_w \end{bmatrix} u_k \tag{21}$$

where Δ is the q_m sampling rate and a_w *and* b_w are the defining parameters of a first order Gauss-Markov (GM) process, The GM process describes the cone bearing acceleration and w_k is white Gaussian noise with zero mean and unit variance.

2.4 *Measurement model*

Currently two synthesized measurements are incorporated into the q_m*KF* algorithm: 1) The best fit seventh degree polynomial to the q_m profile and 2) Output after applying a fourth order low pass frequency filter to the q_m profile. At a later date it is envisioned that additional measurements could be incorporated into the q_m*KF* algorithm as previously described.

$$\begin{bmatrix} z_1 \\ z_2 \end{bmatrix} \equiv \begin{bmatrix} seventh\ order\ polynial\ best\ fit \\ output\ after\ applying\ low\ pass\ filter \end{bmatrix} \tag{22}$$

A best fit 7^{th}degree polynomial is made to the q_m measurements every 1m to 1.4 m depth increment (allowed to be refined by investigator based upon data under analysis) so that the anomalous and spurious peaks and troughs are minimized. This polynomial is then fed into the q_m*KF* algorithm as a measurement. The order of the polynomial and depth increment were selected due to the averaging/blurring of the q_m measurements where it would be highly unlikely that there would be greater than 6 turnings[1] in a 1m to 1.4m depth increment. This assumption was tested with extensive test bed simulation.

A 4^{th} order 250Hz to 300 Hz (allowed to be refined by investigator based upon data under analysis) Butterworth low pass frequency filter is applied to the q_m measurements measurement so that the anomalous and spurious peaks and troughs are minimized even further. This 250Hz low passed frequency filtered trace is then fed into the q_mKF algorithm as a measurement.

1 The maximum number of turnings of a polynomial function is always one less than the degree

3 IMPLEMENTATION OF $Q_M HMM$ AND $Q_M KF$ ALGORITHMS

3.1 *Test bed simulation*

The performance of the $q_m HMM$ and $q_m KF$ algorithms were evaluated by carrying out challenging test bed simulations. This section outlines one of those simulations.

Figure 4 illustrates a simulation of thin bed layering (0.2m) where there is alternating true q_v values of 30MPa and 90MPa (light grey trace) interbedded within a 50 MPa background layer. As is shown in Figure 3 there is a resulting oscillation averaged/smooth q_m trace (black trace) with no sharp peaks or troughs. The output (black dotted trace) of the $q_m HMM$ algorithm is also illustrated in Figure 4. It shall be obvious that the $q_m HMM$ algorithm performed well as the derived $q_v^{/}$ values closely matched the originally specified q_v values.

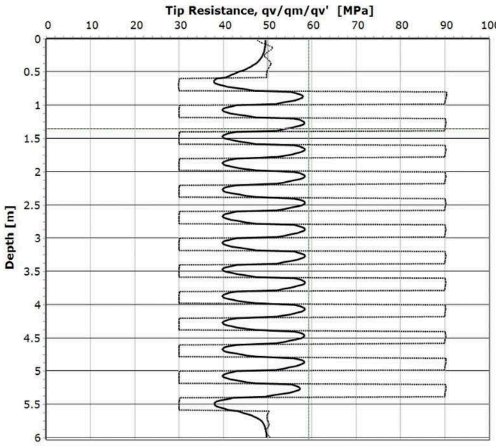

Figure 4. Simulated true cone bearing measurements q_v (light grey trace) and corresponding averaged/blurred q_m (black trace) measurements. The $q_m HMM$ estimated $q_v^{/}$ trace (black dotted trace) is superimposed upon the true cone bearing values.

Figure 5 illustrates the simulated q_m data of Figure 4 (black) with additive noise to represent anomalous/spurious q_m data (red trace). The spurious data was simulated with Gauss-Markov process noise (Baziw and Verbeek, 2021b) with a variance of 60 and time constant of 0.1. The simulated Gauss-Markov noise then had a 250Hz high pass filter applied.

Figure 6 illustrates the estimated q_v (black dotted) trace from the $q_m HMM$ algorithm after processing the output of the $q_m KF$ algorithm (blue trace) of Figure 5. Superimposed on these traces is the true q_v (light grey) trace of Figure 4. As is evident from Figure 6, the combination of the *qmKF* and *qtHMM*

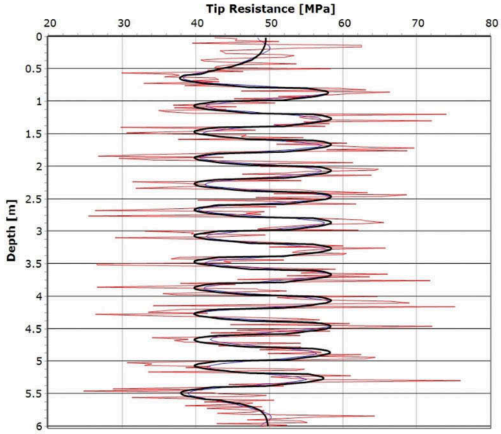

Figure 5. Simulated cone bearing averaged/blurred q_m (black trace) of Figure 3, spurious q_m trace (red trace) feed into the $q_m KF$ algorithm, and the $q_m KF$ algorithm output (blue trace).

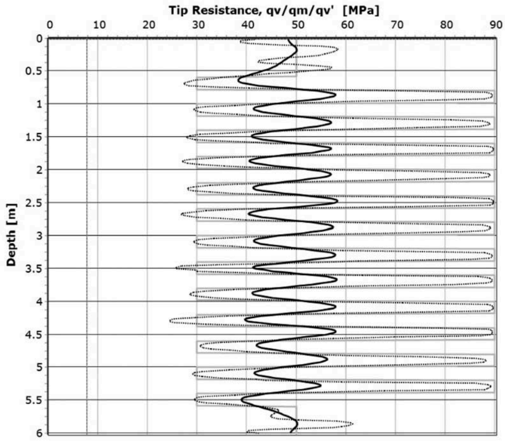

Figure 6. Simulated true cone bearing measurements q_v (light grey trace) and corresponding averaged/blurred q_m (black trace) measurements. The $q_m HMM$ estimated $q_v^{/}$ trace (black dotted trace) is superimposed upon the true cone bearing values.

algorithms results in obtaining impressive estimates of true q_v values from challenging q_m data sets.

3.2 *Real data examples*

After extensive test best analysis, the $q_m KF$ and $q_m HMM$ algorithms were evaluated implemented on real data sets. Figures 7a, 7b and 7c show q_m profiles acquired by Perry Geotech Limited located at Tauranga New Zealand. It is clear from the results presented in these figures that the effect of averaging/

smoothing of the true q_v values (eq. (1)) can results in a significant reduction in the recorded peaks of q_v values, which may very well impact the design based on the CPT data. The q_mKF and q_mHMM algorithms significantly minimize or undo this effect.

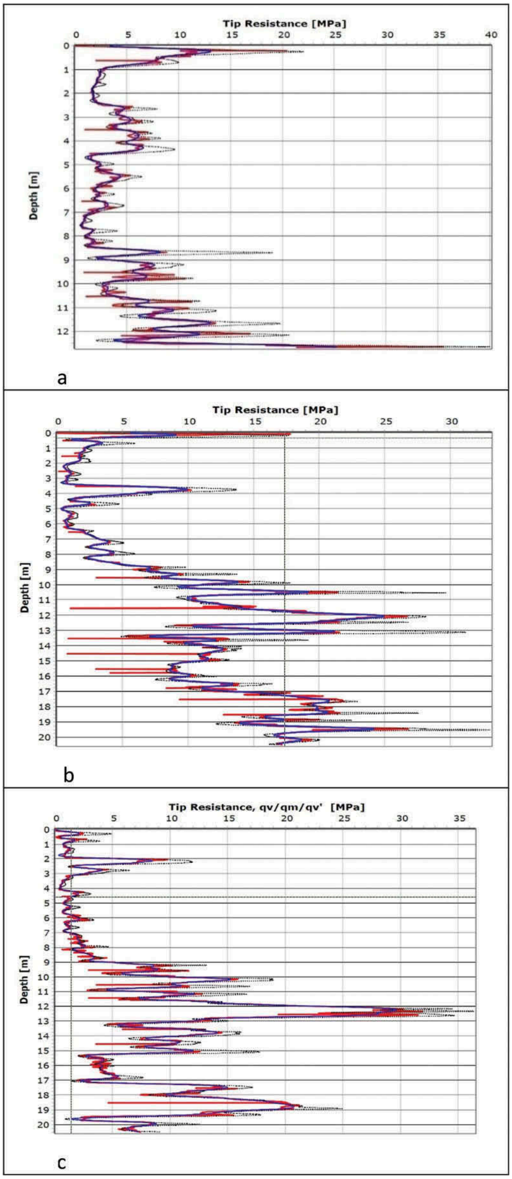

Figure 7. Real data sets. q_m (red trace), output from q_mKF (blue trace) and q_mHMM estimated $q_v^{/}$ trace (black dotted trace).

4 CONCLUSIONS

The q_mKF and q_mHMM algorithms outlined in this paper can effectively minimize the anomalous and spurious peaks and troughs to provide a more accurate depth profile of the cone tip resistance.

By applying these algorithms CPT will provide a more realistic soil behavior profile and also allow for more accurate identification of thin layers. In turn it will provide more accurate input data for any design process that uses the CPT results as direct input.

REFERENCES

ASTM D6067/D6067M – 17 (2017), "Standard Practice for Using the Electronic Piezocone Penetrometer Tests for Environmental Site Characterization and Estimation of Hydraulic Conductivity", ASTM Vol. 4.09 Soil and Rock (II): D5877-latest.

Arulampalam, M.S., Maskell, S., and Clapp, T. 2002. A tutorial on particle filters for online nonlinear/non--Gaussian Bayesian tracking. IEEE Transactions on Signal Processing, vol. 50, no. 2, 174–188.

Baziw, E. and Verbeek, G. 2021a. Cone Bearing Estimation Utilizing a Hybrid HMM and IFM Smoother Filter Formulation. Accepted for publication within the International Journal of Geosciences (IJG) Special Issue on Geoscientific Instrumentation, Methods and Data Systems.

Baziw, E. and Verbeek, G. 2021b. Implementation of Kalman Filtering Techniques for Filtering CPT Cone Bearing Measurements. Accepted published in the DFI 46th Annual Conference on Deep Foundations conference proceedings. October 12-15, 2021 - Las Vegas, NV.

Boulanger, R.W. and DeJong, T.J. 2018. Inverse filtering procedure to correct cone penetration data for thin-layer and transition effects. Proc., Cone Penetration Testing 2018, Hicks, Pisano, and Peuchen, eds., Delft University of Technology, The Netherlands, 25–44.

Gelb, A. (1974). *Applied Optimal Estimation* (4th Edition). Cambridge, Mass: MIT Press.

Lunne, T., Robertson, P.K., and Powell, J.J.M. 1997. *Cone penetrating testing: in geotechnical practice*. Taylor & Francis.

Robertson, P.K. 1990. Soil classification using the cone penetration test. Canadian Geotechnical Journal 27 (1), 151–158.

Robertson, P.K. 1990. Soil classification using the cone penetration test. Canadian Geotechnical Journal 27 (1), 151–158.

Tjelta, T. I., Tieges, A.W.W., Smits, F.P., Geise, J.M., and Lunne, T. 1985. In-Situ Density Measurements by Nuclear Backscatter for an Offshore Soil Investigation. Proc. Offshore Technology Conference, Richardson Texas, Paper No 40917